SEISMIC ON FLOATING ICE:

DATA ACQUISTION VERSUS FLEXURAL WAVE NOISE

Tor Arne Johansen[1,2,3], Bent Ole Ruud[1,2], Ronny Tømmerbakke[1,2] and Kristian Jensen[1]

1) Department of Earth Science, University of Bergen, Norway
2) Research Centre for Arctic Petroleum Exploration, ARCEx, The Arctic University of Norway, Norway
3) The University Centre in Svalbard, Longyearbyen, Norway

Corresponding author: Ronny Tømmerbakke, e-mail: ronny.tommerbakke@uib.no

ABSTRACT

Geophysical surveying of the Arctic will become increasingly important in future prospecting and monitoring of the terrestrial and adjacent areas in this hemisphere. Seismic data acquired on floating ice are hampered with extensive noise due to ice vibrations related to highly dispersive ice flexural waves generated by the seismic source. Several experiments have been conducted on floating ice in van Mijenfjorden in Svalbard in the Norwegian Arctic to specifically analyse the extent of flexural waves recorded with various seismic receivers and sources deployed both on top of ice and in the water below. The data

This article has been accepted for publication and undergone full peer review but has not been through the copyediting, typesetting, pagination and proofreading process, which may lead to differences between this version and the Version of Record. Please cite this article as doi: 10.1111/1365-2478.12756.

show that flexural waves are severely damped at 5 m or deeper below the ice and hydrophone data suffer less from these vibrations compared with data recorded on the ice. Aliasing of single receiver hydrophone data can to some extent be suppressed by using an in-line line source of detonating cord. Experiments on ice on shallow water show prominent guided wave modes often referred to as Scholte waves propagating along the seabed. In this case both flexural and Scholte waves interfere and make a complicated pattern of coherent noise. On shallow water the positioning and type of the seismic source must be evaluated with respect to the coherent noise generated by these waves. Geophone strings of 25 meters effectively suppress both flexural and Scholte waves due to their relative short wavelengths. An airgun generates relative more low-frequency energy than a surface source of detonating cord. Accordingly, seismic mapping of deep seismic horizons seem to be best achieved using geophone strings of such length and an airgun source. For shallow targets, the use of hydrophones in combination with detonating cord is an appropriate solution. Seismic surveying in the Arctic always have to follow environmental restrictions of not disturbing or harming wildlife and not causing permanent footprints into the vulnerable tundra, which implies that the choice of seismic acquisition strategy might occur as a trade-off between optimum data quality and environmental constraints.

Keywords: Flexural wave, Noise, Seismic acquisition

INTRODUCTION

The Arctic has become of increased interest both for seismic exploration but also for monitoring the effect of an altering Cryosphere caused by the ongoing heat flux into this hemisphere. For operational and environmental reasons, acquisition of seismic data during wintertime with frozen grounds might be preferred to the summer season where an acquisition will leave large footprints in the terrain. Analysis of seismic data acquired on floating ice is challenging due to the impact of ice flexural waves generated by the seismic source. These waves are of high amplitude, low velocity with severe dispersion and mask the primary information to be used for seismic imaging. Methods to suppress the influence of this coherent noise, either during acquisition or processing, have been addressed for several decades. In addition, when the seismic acquisition is on ice on shallow water slowly propagating guided waves at the seabed, so called Scholte waves, are also recorded. The Scholte and flexural waves will interfere with the sea bed and further complicate the nature of the coherent noise in the seismic data.

Seismic surveying on top of the ice surface was performed in the ‘50s, ‘60s and ‘70s on a small scale, i.e. zero offset acquisition, during ice drift expeditions by USA (Hunkins 1960), Russians in the Soviet era (Romanov, Konstantinov and Kornilov 1997) and recently by Kristoffersen et al. (2016). A larger research project on land-fast, ungrounded ice has also been done in Beaufort Sea, Alaska with the aim of hydrocarbon exploration (Davidson et al. 2008). Various smaller acquisition tests have also been performed at various locations in order to study the effects of flexural waves in sea ice in North American Arctic (Lansley, Eilert and Nyland 1984; Hall et al. 2001), Antarctic (Sunwall, Speece and Pekar 2012), Russia (Khaidukov 2007) and Svalbard (Johansen et al. 2003, 2011).

The phase velocity of flexural waves increases with frequency but will always be less than the acoustic velocity of water. The velocity depends strongly on the ice thickness and the elastic properties of the ice. For the seismic surveys we have performed on a few months old sea ice less than a meter thick, we find that the flexural waves are mainly confined to a fan constrained by the air wave and zero offset, but in surveys with vibrator as energy source (Beresford-Smith and Rango 1988; Lansley et al. 1984) the flexural waves have been observed to travel faster and thus cover a larger part of the shot gathers. Different techniques have been investigated both in acquisition (Proubasta 1985) and processing (Barr, Nyland and Sitton 1993; Beresford-Smith and Rango 1988; Henley 2006; Del Molino et al. 2008; Khaidukov et al. 2016) specifically aimed to attenuate the flexural wave. Modelling has been performed to look at the effect of various sources (Rendleman and Levin 1990) and also to derive (Press and Ewing 1951a) and model the flexural wave itself (Yang and Yates 1995; Rovetta et al. 2009b).

We here study seismic noise caused by flexural waves generated using explosives on top of the ice or an airgun below, and recorded using single geophones and strings of geophones on the ice surface and hydrophones at different water depths below. The main objective is to reveal possible seismic survey designs which minimize the extent of this noise during data acquisition. The seismic data studied here were acquired during three winter seasons in the inner part of van Mijenfjorden, Svalbard in the Norwegian Arctic. The locations are shown in Figure 1. The time and locations of the experiments were chosen so that both water depth and ice conditions to some extent were different. Flexural waves

were generated using detonating cord exploding on top of the ice and air gun fired at various water depths below. The detonating cord was deployed to form either a point or line source.

We first introduce the basic equations and properties of flexural waves with reference to an example from our data. Subsequently, we review the experimental work and examine data for various acquisition designs and discuss possible ways to dampen the influence of the flexural waves.

PROPERTIES AND MODELLING OF FLEXURAL WAVES

Vibrations in floating sea ice caused by a seismic source excited on the surface of ice, or in the water close below, were first studied both theoretically and experimentally by Ewing, Crary and Thorne (1934), Ewing and Crary (1934) and Press and Ewing (1951a,b). Their theoretical approach is based on the fundamental work of Lamb (1889, 1917) stating that a point or line source causing a vertical displacement within a thin, infinite, fully elastic and isotropic plate in vacuum, excites two fundamental wave modes: one symmetric and one anti-symmetric, also known as extensional and flexural waves. Viktorov (1967) further showed in a plate of a certain thickness at a certain frequency there can exist a finite number of symmetrical and anti-symmetrical Lamb waves, differing from one another by their phase and group velocities and distribution of the displacements and stresses throughout the thickness of the plate. The cut-off frequencies for the zero-order extensional and flexural wave are both zero, whereas the higher-order modes appear outside the normal seismic frequency range and are of no interest in this study. Press and Ewing (1951a) derived the modified vibrations as the elastic plate is resting on a non-viscous fluid and with vacuum above. A third wave

mode occurs if an SH-wave source is applied in the ice, causing an interference pattern of multiple reflected SH-waves referred to as Love waves (Press and Ewing 1951a).

In our experiments, the thicknesses of ice are less than one meter, which implies that for seismic frequencies and common wave velocities in ice, the wavelengths of the propagating waves along the ice sheet are much larger than ice thickness. In the case of vacuum on both sides, the velocity V_e of the extensional wave is independent of ice thickness and given by (Press and Ewing 1951a):

$$V_e = \sqrt{\frac{E}{\rho(1-\sigma^2)}}, \tag{1}$$

where E, σ and ρ are the Young's modulus, Poisson's ratio and density of the ice. In the similar case, the phase velocity $V_{fl\text{-}P}$ of the flexural wave is (Cremer, Heckl and Petersson 2005)

$$V_{fl-P} = \sqrt[4]{\frac{D}{\rho H}}\sqrt{\omega}, \tag{2}$$

where ω is angular frequency, H is ice thickness and D is the plate bending stiffness defined by

$$D = \frac{EH^3}{12(1-\sigma^2)}. \tag{3}$$

As seen from equation (2) the flexural wave is highly dispersive and has very low velocities for low frequencies. Since the extensional wave mode have mainly horizontal displacement, the interaction with the fluid is weak, and the effect of the water layer has by Press and Ewing (1951a) been shown to result in a phase velocity with a small imaginary component, which hardly affects its velocity. Since its phase velocity is larger than the water velocity, it will generate a downward propagating wave in the water, resulting in some attenuation.

The vertical displacement of the flexural waves causes strong interaction between ice and water. Yang and Yates (1995) analyzed flexural waves for ice sheets resting on water and with vacuum above. They consider the waves to be of low-frequency when the phase velocity of the same ice sheet with vacuum at both sides is less than the acoustic velocity of air. From (2) we see this means that:

$$\omega \leq V_{Pa}^2 \sqrt{\rho H / D}, \tag{4}$$

with V_{Pa} denoting the P-wave velocity in air. The dispersion relation of the flexural wave with wavenumber k and frequency ω, hence $V_{p\text{-}fl}=\omega/k$, in case of deep water (water half-space) is following Yang and Yates (1995) given by:

$$\Omega(k) = \left(k^4 - k_f^4\right)\left(k^2 - k_w^2\right)^{\frac{1}{2}} - \frac{\rho_s}{\rho_w H} k_f^4 = 0, \tag{5}$$

where

$$k_w = \omega / V_{Pw}. \tag{6}$$

V_{Pw} is P-wave velocity in water and k_f denotes the flexural wavenumber when there is no loading effect caused by the water layer, which from equation (2) is

$$k_f = \sqrt[4]{\rho H \omega^2 / D}. \tag{7}$$

Exact solutions of the dispersion relation (5) can only be found numerically as it implies solving a fifth degree polynomial. There is only one real root which corresponds to the physical solution (Crighton 1979).

The group velocity can be derived from the phase velocity, which from equation (5) leads to

$$V_{fl-G} = \omega \frac{\left(k^4 - k_f^4\right)k + 4k^3\gamma^2}{\left(k^4 - k_f^4\right)k_0^2 + 2k_f^4\left(\gamma^2 + {}^{\rho_w\gamma}/_{\rho H}\right)}, \quad (8)$$

where $\gamma = \sqrt{k^2 - k_w^2}$ (note that we always have $k > k_w$ for flexural waves). The phase velocity of the flexural waves is usually much less than the water velocity, thus $k^4 \gg k_w^4$, and a good approximation is therefore to set $k_w = 0$ in equation (5) (which is the same as to say that the water is incompressible). After some simple mathematical manipulations, and combining with equations (1) – (3), we arrive at the following equation:

$$V_{fl-p}^2 = \frac{1}{12}\frac{\rho V_s^2 (kH)^3}{\rho_w + \rho kH}. \quad (9)$$

This result is equivalent to the low-frequency approximation derived by Press and Ewing (1951a), and can be used to compute the phase velocity of the flexural wave for a given wavenumber. By setting $\rho_w = 0$ we see that equation (9) is also consistent with equation (2) for a plate in vacuum. Note that the velocities of both the extensional and the flexural waves depend on the same combination of elastic properties $\left(\frac{E}{1-\sigma^2}\right)$ and thus prevents us from resolving any other elastic properties of the ice by observing only these two wave types. An overview of the change in phase velocities for extensional and flexural waves can be seen in Figure 2.

Figure 3 shows schematics of the various experimental setups used for acquiring data in this study, and which in combination with Table 1 provides necessary details of the experiments E1 – E17. To estimate ice properties, we performed a shear velocity measurement (E1) where a solid, stiff plate of steel was mounted and frozen vertically into the ice and in inline direction as shown in Figure 4a. A sledgehammer was used as source, mainly generating SH waves but also some P wave

energy, which were recorded on 3-component geophones as shown in Figure 4b. The velocity of an SH wave is given by

$$V_{SH} = \sqrt{\frac{\mu}{\rho}} = \sqrt{\frac{E}{2\rho(1+\sigma)}}, \quad (10)$$

which when combined with equation (1) gives

$$\sigma = 1 - 2\left(\frac{V_{SH}}{V_s}\right)^2. \quad (11)$$

In our case we measured $V_s = 1650$ m/s and $V_{SH} = 980$ m/s which gives $\sigma = 0.28.$ Assuming an ice density of 920 kg/m^3, we can compute Young's modulus from (1) as $E = 2.7$ GPa. The P-wave velocity is given by

$$V_p = \sqrt{\frac{E(1-\sigma)}{\rho(1+\sigma)(1-2\sigma)}}, \quad (12)$$

which can be combined with (1) to give

$$\frac{V_P}{V_s} = \frac{1-\sigma}{\sqrt{1-2\sigma}}, \quad (13)$$

and we find $V_p = 1.8$ km/s. Since we assume an isotropic ice layer, the S-wave velocity is the same as for the SH-wave. We note from equation (11) that estimation of the Poisson ratio is quite sensitive to measurement errors in V_{SH} and V_s, so that the uncertainties in Young's modulus and V_p become quite large.

When elastic properties derived from the extensional and flexural wave differ as will be shown below, this indicates that the elastic properties within the ice vary in the vertical direction, for example due to layering. The ice was during the 2013 campaign made up by a very soft, slushy bottom layer and a much stiffer upper layer. Figure 5a shows shot gather from E2 where the flexural waves generated from a point source mask the data in a fan spanned by zero offset to a line just

exceeding the linear air wave event. An explosion on top of ice produces a relative strong air wave guiding the flexural wave. The gather also displays the dispersive nature of the flexural waves with low velocities at low frequencies approaching the air wave velocity for the higher frequencies. Also indicated is the extensional wave having a velocity of about 2370 m/s. Figure 5b displays phase velocity versus frequency estimated from the same shot gather. In order to match the observed dispersion curves for the flexural wave, the velocity of the extensional wave had to be considerably lowered. Theoretical curves using equations (2) and (9) are included, but now using the values V_e=1667 m/s and σ=0.33 and assuming ρ=920 kg/m^3. A likely explanation for the lowered value of V_e used to match the dispersion relation is that the ice sheet is layered, with lower Young's modulus in the lower part. Looking at the modelled dispersion curves we see vacuum above ice and water below (eq. (9)) match the data well, while with vacuum on both sides (eq. (2)) the phase velocities are much higher. The flexural waves in the ice are slowed down because they must displace the water below (the effect is similar to an increase in the surface density of a plate in vacuum, except from the frequency dependency). Figure 6 shows the seismic wave field from experiment E3 on a spread orthogonal to the in-line direction also including modelled travel time curves of the extensional wave, air wave and for some frequencies of the flexural wave using equation (8).

Synthetic seismograms of flexural waves based on the parameters describing the ice conditions (thickness and its elastic properties) can be modelled using the dispersion relation in equations (5) or (9), following the procedure described by Yang and Yates (1995). The seismograms are constructed in the space-frequency (x, ω) domain and thereafter Fourier transformed to the space-time (x,t) domain. Considering a point source with Fourier spectrum $F(\omega)$, the synthetic seismogram of the vertical displacement at distance x from the source point can be obtained by numerically evaluating

$$s(x,t) = \frac{1}{D}\int_{-\infty}^{+\infty} \frac{iF(\omega)\gamma H_0^{(1)}(kx)k}{d/dk[\left(k^4 - k_f^4\right)\gamma - \mu k_f^4]_{k=k_1}} e^{-i\omega t}\, d\omega, \quad (14)$$

where k_1 is the real root of equation (5) and $H_0^{(1)}$ is the Hankel function of zeroth order and first kind.

Figure 7 displays a modelled synthetic seismogram of the flexural waves using the dispersion relation of Figure 5b based on equation (14) and the source function is the impulse response of a 4-8 Hz second order Butterworth bandpass filter. Compared with Figure 5a, we see that the modelling gives a very similar wave pattern as the real data except for the effects caused by the air wave and that the source signatures are different. Such modelling provides a realistic diagnostic of the noise problem caused by the flexural waves when ice properties are known and the water depth is large. Furthermore, a synthetic flexural wave seismogram can be used as *a priori* input for adaptive-subtractive noise removal from real data as shown by Rovetta et al. (2009a,b).

CONVERSION OF GEOPHONE AND HYDROPHONE DATA

In order to compare or combine data from geophones on ice and hydrophones in water, we need to convert the measurements to a common physical unit. The geophones measure particle velocities, while hydrophones measure pressures. The flexural wave in ice causes evanescent waves, with amplitudes decreasing downward into the water, while the reflected and refracted waves from the subsurface impedance contrasts are propagating waves going upward, or in case of Scholte waves, evanescent waves with amplitudes decreasing upward. Since the ice is much thinner than the wavelengths of the seismic waves, we assume that the vertical displacements on top and bottom of the ice as well as in the water at the ice/water boundary are all equivalent.

Consider a 2 dimensional model where x and z are coordinates along horizontal and vertical (downward pointing) axes, respectively. For a plane wave propagating downwards in the water at an angle θ from the vertical, the pressure can be written

$$P = A(\omega)\exp[i\omega(px + qz - t)], \tag{15}$$

where the horizontal and vertical components of the slowness vector are given by

$$p = \frac{\sin\theta}{V_w}, \quad q = \frac{\cos\theta}{V_w} = \left(\frac{1}{V_w^2} - p^2\right)^{\frac{1}{2}}, \tag{16}$$

respectively, and $A(\omega)$ is the Fourier transform of the pressure wavefield. The equation of motion is

$$\rho_w \frac{\partial \vec{v}}{\partial t} = -\nabla P, \tag{17}$$

where $\vec{v}$ is the particle velocity vector. In the frequency domain this becomes $i\omega\rho_w v_z = \frac{\partial P}{\partial z}$ for the vertical component. From (15) we also find $\frac{\partial P}{\partial z} = i\omega q P$ which we can combine with the equation of motion to give

$$P = \frac{\rho_w}{q} v_z. \tag{18}$$

If we replace q with its definition from (16), we get $P = \rho_w V_w / \cos\theta \, v_z$, which we recognize as the relation between pressure, acoustic impedance $\rho_w V_w$, and particle velocity for vertical wave propagation (Aki and Richards 1980). For $p > 1/V_w$, q is imaginary and the pressure wave is evanescent. The angle θ will become complex, and therefore the form in (18) is more convenient to use. It is important to note that (18) was derived for a single plane wave as given by (15). Thus we cannot use (18) unless we can decompose the wavefields into plane waves. For evanescent waves

the sign of q is imposed by the radiation condition which requires decreasing amplitudes for increasing z, thus q must be positive imaginary. If we solve (18) for v_z, we find that it is proportional to q. Using (15) and (17) we can perform a similar derivation to find that v_x is proportional to p, which is real. This means that the vertical component will have a phase delay of π/2 radians relative to the horizontal, and thus the particle motion in water must be prograde elliptical.

The boundary condition for the vertical displacement (and for the vertical particle motion) requires continuity at the ice/water interface. The flexural wave propagates along the horizontal axis and causes only vertical displacements and thus we assume that at the ice/water boundary the values of v_z are equivalent to those measured by geophones on top of ice. Snell's law assures invariant horizontal wave slowness for wave transmission across horizontal boundaries and we can define $p = 1/V_{fl-p}$. Equation (16) infers that the vertical slowness of the flexural wave in water becomes imaginary since its velocity in our case is always less than the P-wave velocity in water. Furthermore, since flexural wave velocity is highly frequency dependent, so is the vertical slowness in water, consequently equation (16) becomes

$$q(f) = i\left(\frac{1}{V_{fl-P}^2(f)} - \frac{1}{V_w^2}\right)^{\frac{1}{2}}, \tag{19}$$

which also implies that the relation between pressure and vertical particle velocity in equation (18) becomes frequency dependent. By combining equations (18) and (19) we see that in order to convert particle velocity on ice to fluid pressure in water just below implies a negative phase shift of $\pi/2$ radians and a frequency dependent amplitude scaling as governed by equation (19). It is important to notice that the calibration filter depends on the ice properties at the time of data acquisition. Since the phase velocity of flexural waves is usually much lower than the acoustic

velocity in water, a good approximation is $q(f) = i/V_{fl-p}(f)$. From equation (9) we see that when the wavelength is much less than the ice thickness (kH << 1), $V_{fl-p}(f)$ is proportional to $f^{3/5}$, and thus the frequency dependent part of the conversion filter also becomes proportional to $f^{3/5}$. This can be compared to Barr et al. (1993) who find that the conversion filter is simply a time derivative (multiplication with 2πif in the frequency domain).

Since the flexural wave, for seismic frequencies, consists of a single mode, all the energy at a given frequency will be confined to a single slowness component. Consequently, if the pressure in the water due to the flexural wave is known at a point (x_1, z_1) we can extrapolate the pressure field to any other point (x_2, z_2) with a simple formula which for a 2D model is

$$P(f, x_2, z_2) = P(f, x_1, z_1) e^{2\pi i f (p(x_2 - x_1) + q(z_2 - z_1))}. \quad (20)$$

Obviously, for this to work in practice, there must be no significant interference from other types of waves, or the flexural wave must have been separated from the other waves by some kind of plane wave decomposition. For 3D models we should also include a correction for the cylindrical spreading in equation (20). Since *p* is always real and *q* is always imaginary, equation (20) means that pressure amplitudes of the flexural wave will decay exponentially with depth, while they propagate with no attenuation horizontally (time domain amplitudes will still decrease with increasing offset due to dispersion). This will be further emphasized in the experimental data shown in next section.

EXPERIMENTAL DATA

Our experiments were specifically designed to evaluate the extent and nature of flexural waves in shot gathers for various source and receiver configurations. The flexural waves were generated using either detonating cord on the ice surface or an air gun in the water at various depths below the ice. Ice conditions and water depths varied as listed in Table 2.

The amplitudes of the flexural wave will decay exponentially with depth which is according to equation (20) and it is of interest to evaluate the extent of flexural waves in hydrophone data from various depths compared with their appearance in geophone data. Figure 8 shows data from experiments E4 to E7 which clearly reveals the increased damping of the flexural wave amplitudes with increasing hydrophone depth. At 5m depth or approximately 4.3 m below the ice, the flexural wave is almost absent. The main noise event is caused by the air wave. At 10 m depth the air wave is still clear, while at 20 m depth it is weak and there are no signs of the flexural wave. This observation suggests that using hydrophone receivers 5 - 10 m below the ice will only to a small extent be influenced by the flexural waves. A downside is loss of the spatial anti-alias filtering by using single hydrophone receivers versus geophone strings.

To compare and calibrate the flexural wave in geophone data with hydrophone data, we used the dispersion relation obtained from the data in Figure 5b as input to equations (18) and (19) to design an appropriate filter. A trace of geophone, hydrophone and converted geophone data are shown in Figure 9. The residual trace of the hydrophone and converted geophone data is also included, showing that the filtering works well. According to Parrish, Palm and Bell (2015) the hydrophone response might show frequency and phase variations and individual calibration might improve the filtering. The calculated pressure data is essentially a slight high-pass filtering of the

geophone data in addition to a phase shift of $\pi/2$ radians. Barr et al. (1993) discussed this phase shift, which is of opposite sign for flexural and P waves, as a possibility to phase shift hydrophone data using a Hilbert transform so that primary upgoing waves in geophone and hydrophone data become coherent while the flexural waves become of opposite polarity (π radians out of phase). A stack of the geophone and the phase-shifted hydrophone data will then reduce the impact of the flexural wave. Barr et al. (1993) did however discard the amplitude scaling caused by the dispersion of the flexural wave.

The flexural wave of the geophone to hydrophone converted data can, using equation (20), be extrapolated to other depth values. Figure 10 shows a comparison of a hydrophone gather at 1 m depth extrapolated to 5 m depth. Since the extrapolation filter was specifically designed for the flexural wave we do not expect that the reflected and refracted waves to be comparable.

Although hydrophones below ice are effective for reducing the impact of the flexural waves, the use of single receivers makes the system vulnerable for spatial aliasing, which can be reduced using geophone strings on the ice. Deploying detonating cord as an in-line line source will to some extent reduce this problem. Figure 11 shows f-k spectra of both geophone and hydrophone shot gathers obtained using line source (E8 & E9) and point source (E10 & E11) source. As seen, the line source acts as a spatial anti-alias filter whose characteristics are defined by the length of line of detonating cord, but on the price of less seismic resolution. Figure 12 compares two f-k spectra of split-spread shot gathers applying 25 m long detonating cord (E12) or an air gun (E13), and recorded using 12.5 m long geophone strings. By comparing the plots in Figures 11 and 12, we see that the combination of 25 m long source and geophone strings very effectively dampen the flexural wave. An air gun generates more low frequency energy in the seismic frequency range, except for 3-10Hz,

than a detonating cord at the ice surface as seen in Figure 13, which is favorable for seismic imaging of deeper geological strata. Also by using an air gun the air wave event is avoided, but a direct P-wave parallel to the ice sheet is generated.

Our last examples show shot gathers obtained at ice floating on water depths of a few meters. Along the spread the depth of the hydrophones are varying and geophones are placed on top of the ice. Figure 14 shows hydrophone gathers using both detonating cord (E14) and an air gun at 1.5 m (E15). The air gun generates both flexural waves but also a prominent Scholte wave. The flexural waves are now also interfering with the sea bed and give a more complicated noise pattern in the data. The surface source generates more flexural waves but less energy associated with the Scholte wave compared with using an air gun. The geophones on ice will also receive strong Scholte waves with an air gun as source. This is furthermore emphasized in Figure 15 showing geophone shot gathers with the air gun deployed at depths of 1.5 m (E16) and 3 m (E17) (about 3 m above the sea bed). The closer the air gun is to the subsurface of the ice, the stronger is the flexural waves. And, the closer it is to the seabed the stronger is the Scholte waves. This is in accordance with the theory outlined in e.g. Shtivelman (2004).

DISCUSSION

The experiments have addressed a suite of various seismic acquisition set ups on floating ice to obtain a reference of real data which can be used to find survey parameters for obtaining best possible seismic imaging under such conditions. However, a design for mapping the deep structures usually imply degraded data quality for mapping shallow structures and vice versa. Operations in the Arctic are usually underlain severe environmental restrictions constraining when and where to

survey and what type of seismic source to be used (Trupp et al. 2009). At Svalbard, as in many other areas in the Arctic, during late winter/early spring, the breeding seasons of sea mammals will in particular put limitations to the operational procedures. Therefore an optimum survey design will sometimes be bounded by environmental constraints. From an operational point of view surveying during wintertime is favorable since there will be no permanent footprints of the operation on the surface and the stiff surface makes it easier to transport equipment and crew into the field. In periods when the coastal areas are covered by solid ice this give the possibility to survey areas of shallow water which otherwise are very difficult to enter. This provides an opportunity to acquire continuous seismic data to map geological transects from land to sea.

The data obtained give valuable insights in the generation and monitoring of flexural waves on floating ice for various sources as explosives on top of the ice and an air gun in the water below. Single geophones and strings of geophones were placed on top of the ice and hydrophones were deployed at various depths below the ice. Furthermore, for ice on shallow water, our experiments reveal the extent and nature of Scholte waves. Scholte waves can be used to map sediment thicknesses and properties of the uppermost seabed strata (Kugler et al. 2005; Boiero, Wiarda and Vermeer 2013) .

The hydrophone data reveal that the flexural waves are almost absent at 10 m depth. A surface explosion causes an air wave which still is seen at 10 m depth but almost invisible at 20 m depth. An air gun produces more downward propagating energy in the seismic frequency range compared to surface explosives, but generates a relatively strong direct P-wave. This wave can be of high amplitude in case of shallow water due to reverberations with the sea bed, while its energy decreases as water depth increases. The use of air guns also produces upward propagating energy, reflected downward at the ice bottom joining the original downward as a delayed pulse with

opposite polarity, called ghost. This will add a deghosting processing step in the processing sequence. Deghosting of source and receivers on sea ice is not a subject we investigated in our experiments, but we expect that such a procedure will essentially follow processing steps similar to those used for marine seismic surveys. The effect of the ice layer can be accounted for as described by Barr et al. (1993). To avoid flexural wave energy the use of hydrophones are superior to ice surface geophones, but use of single receivers makes the system more vulnerable to slowly propagating waves which causes spatial aliasing. The use of detonating cord can reduce the amplitude of aliased waves by deploying it as a line source in the in-line direction. The length of the detonating cord defines its array response and accordingly the most suitable length can be designed based on knowledge of ice conditions and water depth.

Strings of gimballed geophones, 25 m long, often used during land seismic surveying, combined with a source of 25 m long detonating cord, shows to effectively dampen the flexural waves when the water depths are more than a few meters. In this case an air gun would provide more downward propagating energy, but at the expense of operation time since drilling holes and deploying air gun are somewhat cumbersome. Alternatively, several shots of detonating cord could be repeated at each position. This implies that a conventional seismic snow streamer surveying as described by Johansen et al. (2011) should also be effective for imaging deeper geological strata on floating ice. For shallow surveying, hydrophones combined with detonating cord should be favorable. Consequently, for potential imaging of the Cryosphere under such conditions a combination of hydrophones and detonating cord should apply. From an operational point of view, this latter seismic set up, severely minimizes amount and weight of equipment and resources needed to perform such surveying.

CONCLUSIONS

We have revealed the main properties of strongly dispersive ice flexural waves from analysis of various seismic experiments on floating ice conducted in the inner part of van Mijenfjord at Svalbard in the Norwegian Arctic. The analysis shows that deploying hydrophones 5 m or more below the ice severely reduces the influence of ice flexural waves. Flexural wave energy is also effectively attenuated by use of 25 m long gimballed geophones strings. Choice of receiver type and source has to be evaluated based on the target depth of the seismic imaging to be undertaken. The length of detonating cord when used as an in-line line source can be designed to reduce the impact of waves which cause aliasing when single receivers are used. In practice, an optimum survey design has to comply with the often serious environmental restrictions imposed on seismic operations in Arctic.

ACKNOWLEDGEMENTS

We acknowledge ENI Norge AS for financial support of fieldworks in 2016 and 2018, and Statoil ASA for financial support of field work in 2013. This study has been carried out in the courtesy of Research Center for Arctic Petroleum Exploration (ARCEx) partners, and the Research Council of Norway (Grant No. 228107). Also, we acknowledge Seabed Geosolutions for access to instrumentation and technical assistance. Finally, we appreciate the constructive suggestions from our reviewers.

TABLES

Experiment	Near Offset (m)	Rcv Type	Spread length (m)	Group distance (m)	Group length (m)	Rcv depth (m)	Source Type	Source strength (kg)	Source depth (m)	Year
1	0	3C	120	4.16	Single	0	S	N/A	0	2016
2	25	GG	750	6.25	6.25	0	PDC	2	0	2013
3	400	GG	750	6.25	6.25	0	PDC	2	0	2013
4	25	H	375	12.5	Single	1	PDC	0.5	0	2013
5	25	H	375	12.5	Single	5	PDC	0.5	0	2013
6	25	H	375	12.5	Single	10	PDC	0.5	0	2013
7	25	H	375	12.5	Single	20	PDC	0.5	0	2013
8	25	GG	375	12.5	12.5	0	DC	25m line	0	2013
9	25	H	375	12.5	Single	1	DC	25m line	0	2013
10	25	GG	375	12.5	12.5	0	PDC	1	0	2013
11	25	H	375	12.5	Single	1	PDC	1	0	2013
12	0	GG	2150	25	12.5	0	DC	25m line	0	2018
13	0	GG	2150	25	12.5	0	A	12 cu.in.	3	2018
14	50	H	350	12.5	Single	1-10	DC	12.5m line	0	2016
15	50	H	350	12.5	Single	1-10	A	30 cu.in.	1.5	2016
16	50	GG	350	6.25	6.25	0	A	30 cu.in.	1.5	2016
17	50	GG	350	6.25	6.25	0	A	30 cu.in.	3	2016

Table 1 Overview experiments E1-E17. Abbreviations used for Receiver (Rcv) Type: 3C – 3 component geophone, GG – Gimballed geophone string and H – Hydrophone. Abbreviations used for Source Type: S – Sledgehammer, DC – Line source detonating cord, PDC – Point source detonating cord and A – Airgun.

Acquisition year	Ice thickness (cm)	Water depth (m)
2013	**74 to 79**	**52 to 60**
2016	**30 to 40**	**7 to 13**
2018	**20 to 40**	**0 to 50**

Table 2 Ice thickness and water depth measured over the acquisition areas.

LIST OF FIGURE LEGENDS

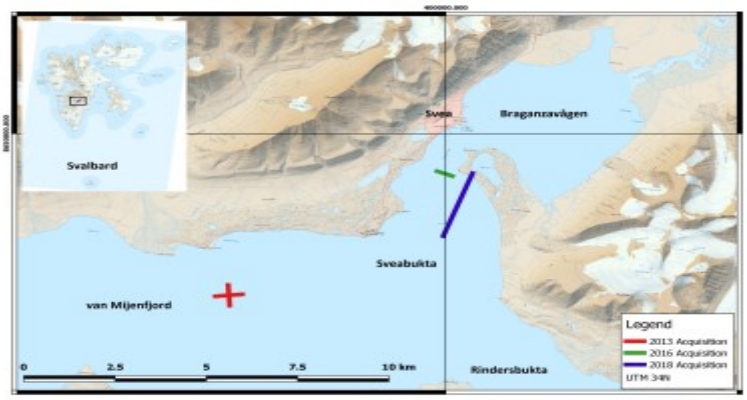

Figure 1. Overview of locations of the various experiments conducted in 2013, 2016 and 2018.

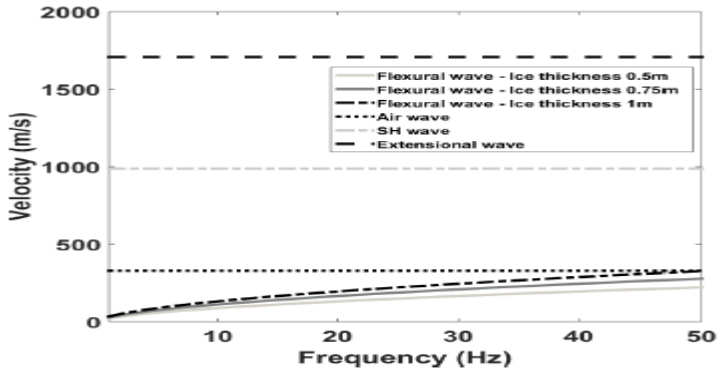

Figure 2. Phase velocity of typical waves seen for seismic experiments on an ice sheet with air above and water below using equation (5) for the flexural wave. Young's modulus set to 2.3 GPa, $\rho = 920\ kg/m^3$ and $\sigma = 0.33$. The velocity of the air wave (330 m/s) is for a temperature of $-2\ C^{\circ}$. Left figure shows 3 different ice thicknesses and the corresponding flexural wave and air wave. Right figure also includes SH (988.2 m/s) and extensional wave (1707.4 m/s).

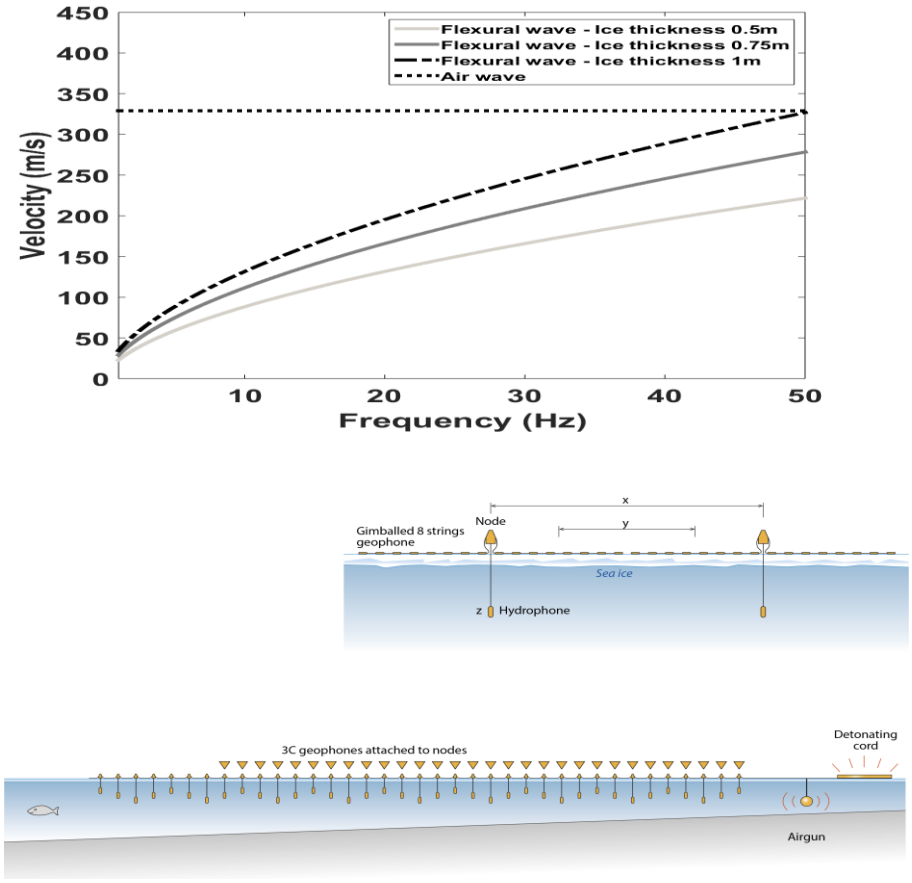

Figure 3. Schematics of experimental seismic set ups. x, y, z denote hydrophone interval, geophone group interval and hydrophone depth, respectively. Lower figure is specific for the 2016 campaign. Note the hydrophone depths varying (1-10m).

Figure 4. a) Steel plate frozen into the sea ice used as shear wave source. b) Data from experiment E1 in Table 1 showing 3-component recordings from a sledgehammer blow transverse to the line. In the upper figure showing the three components at 100 m offset, the components have the same scale, while in the two lower figures the traces have been scaled individually (there are four dead traces on each of the lower figures due to improper coupling of geophones in the setup). The extensional Lamb wave is seen only on the radial (R) component while the much stronger shear-horizontal (SH) wave is seen on both the transverse (T) and radial component. The SH waves on the R component might indicate a small error in the orientation of the 3C geophones.

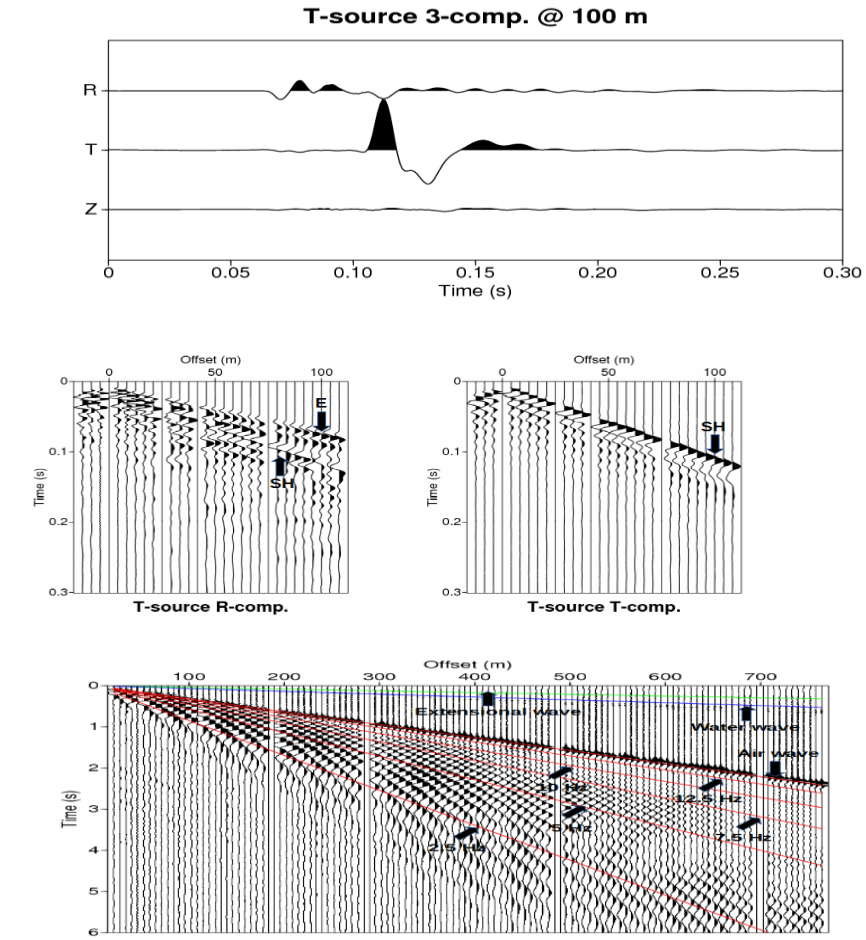

Figure 5. a) Shot gather from experiment E2 with a point source, and b) estimated phase velocity curves from data and the modelled phase velocity of the flexural waves considering ice resting on water (equation (9)), and vacuum (equation (2)) respectively. The coloured lines in a) represent group velocities for various waves: green – extensional wave (2370 m/s), blue – water wave (1450 m/s), red – air wave (317m/s, air temperature $-23\ C^{\circ}$) and flexural waves (293, 258, 220, 175, 118 m/s). The five lowest lines corresponds to the group velocity of the flexural waves for frequencies of 12.5, 10.0, 7.5, 5.0 and 2.5 Hz. The extensional wave is very weak on these vertical component seismograms, and can be seen only when the amplitude scaling is increased.

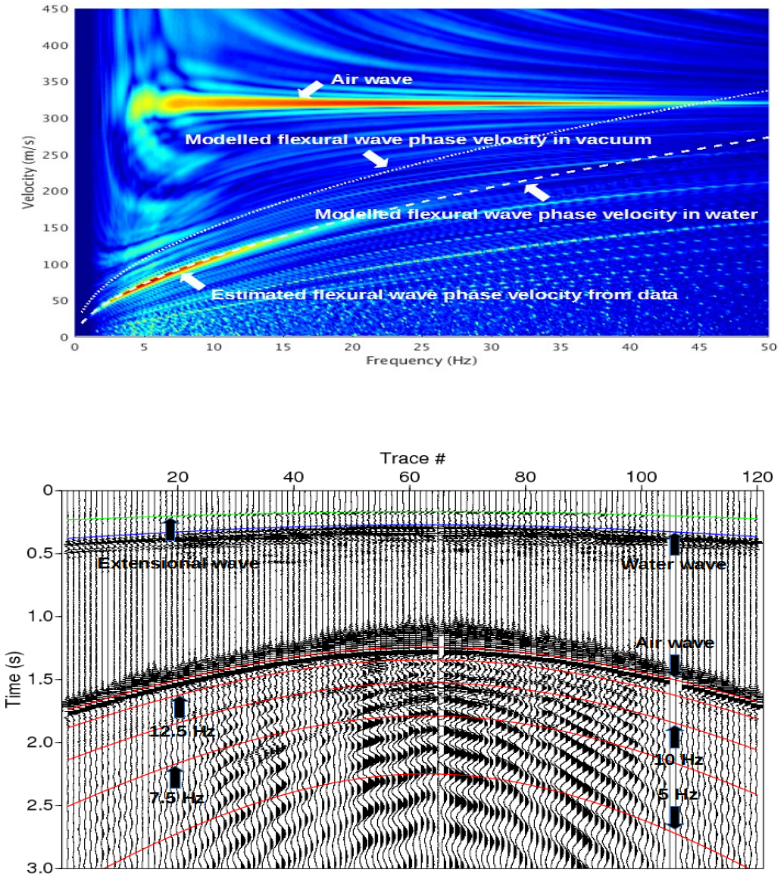

Figure 6. Shot gather from orthogonal spread using a point source (E3) including modelled travel time curves of extensional wave (green), water wave (blue) and air wave (red). The four lowermost curves correspond to flexural wave group velocities of 12.5, 10.0, 7.5, and 5.0 Hz (293, 258, 220, and 175 m/s). For the non-dispersive waves (the extensional wave, water wave, and air wave) the wavefronts are seen to match the curves of constant group velocity. The flexural waves are very dispersive, and therefore the wavefronts (curves of constant phase) do not match the red curves of constant group velocity.

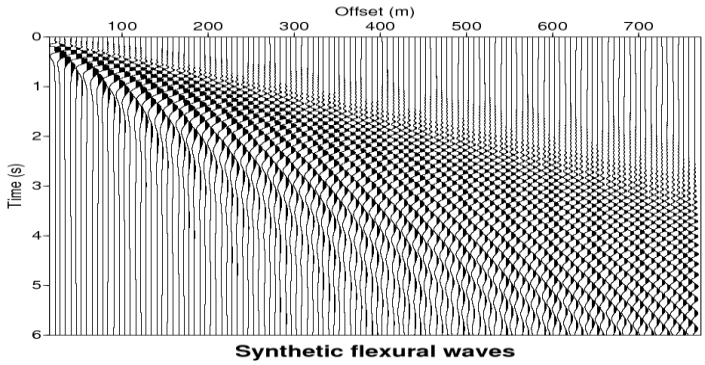

Figure 7. Modelled gather of flexural waves, based on the theory of Yang and Yates (1995) for free waves, using parameters estimated from experiment E2.

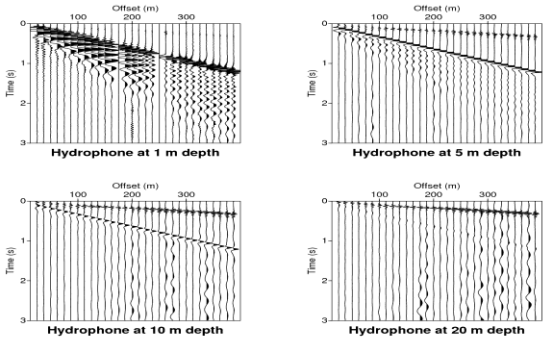

Figure 8. Shot gather using a point source at the ice surface recorded with single hydrophones deployed at various water depths (experiments E4 to E7). The air wave and flexural wave amplitudes are seen to decrease with increasing hydrophone depth while the water wave amplitude increases.

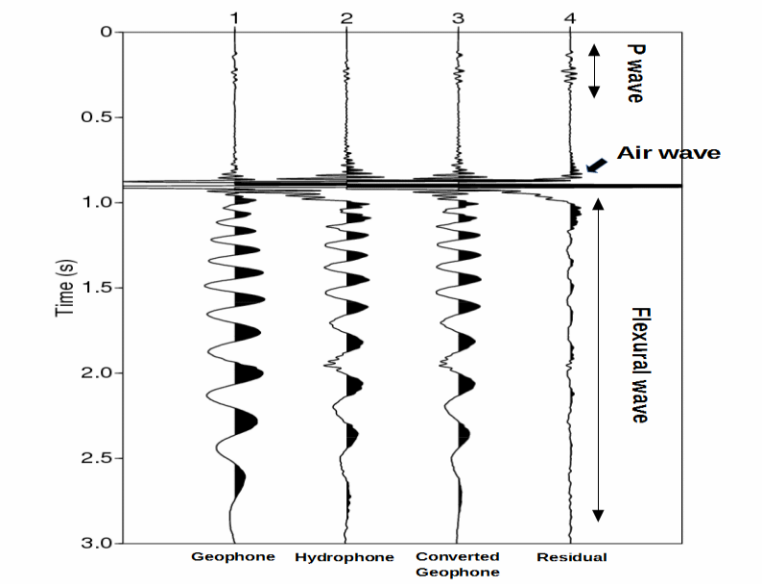

Figure 9. Traces (at 287m offset) with data from (1) single geophone on ice, (2) single hydrophone under ice, (3) geophone trace (1) converted to hydrophone, and (4) the difference between (2) and (3). Both geophone and hydrophone data were converted to SI units, and differences in the instrument responses were removed, before further processing. Traces (2)-(4), which all have units of pressure (Pa), are shown to the same scale. Trace (1), which shows the particle velocity (m/s), have been scaled up with a factor of 10^5 ***relative to the other traces.***

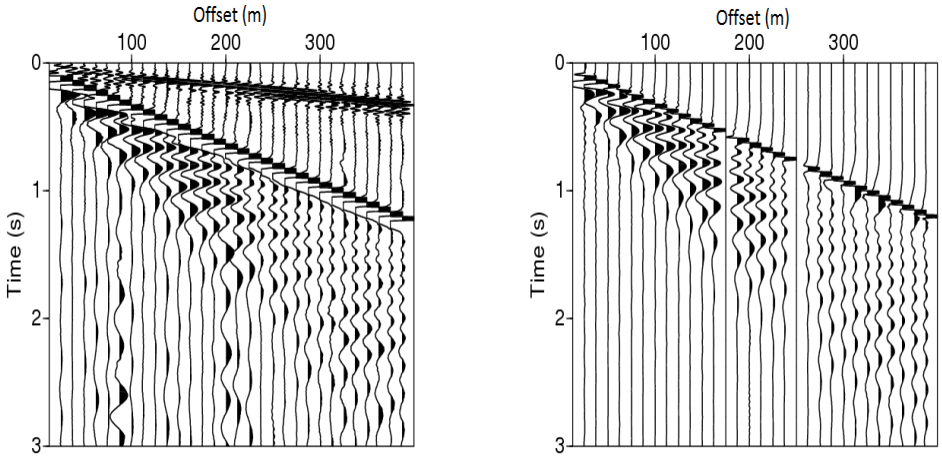

Figure 10. (left) Shot gather recorded with single hydrophones at 5 m depth (E5), and (right) shot gather recorded with single hydrophones at 1 m depth (E4) extrapolated to 5 m depth using equation (20). The two shot gather are shown with the same scaling. The left gather is the same as the hydrophone gather at 5m in Figure 8, but here scaled up with a factor of 4. The flexural wave is seen to scale as expected (the flexural waves have approximately the same strength in the two gathers), while the other waves have been strongly attenuated by the extrapolation process which is essentially a low-pass filter.

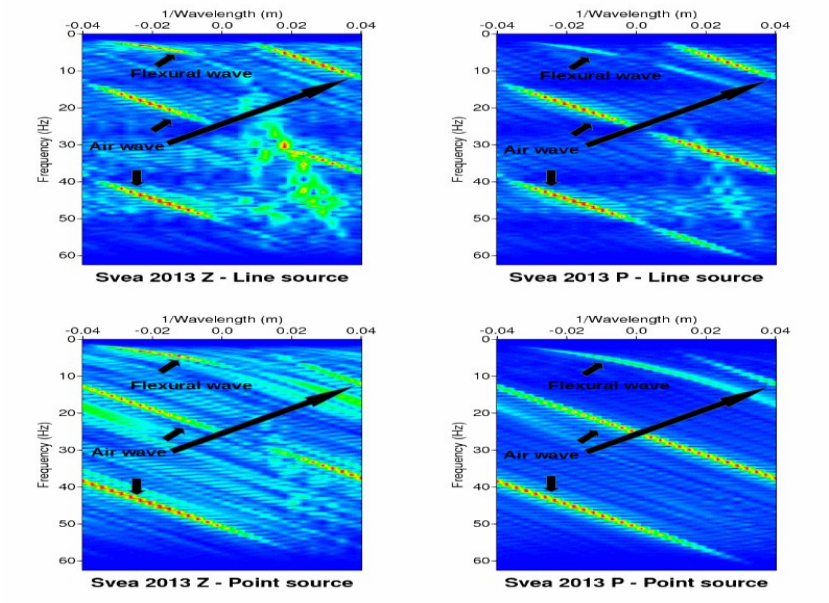

Figure 11. Frequency-wavenumber spectra of shot gathers using a line source (upper figures) and a point source (lower figures) recorded by geophone strings (left figures) and single hydrophones (right figures) (E8-E11). The hydrophone depth was 1 m so the air wave and the flexural waves are seen to be very strong also in the hydrophone data. The length of the line source was 25 m and the length of the geophone strings was 12.5 m. The reflected P-waves are best seen for the shot gathers with a line source and using geophone strings. The shot gather for a point source and point receivers is heavily influenced by the aliased air and flexural waves.

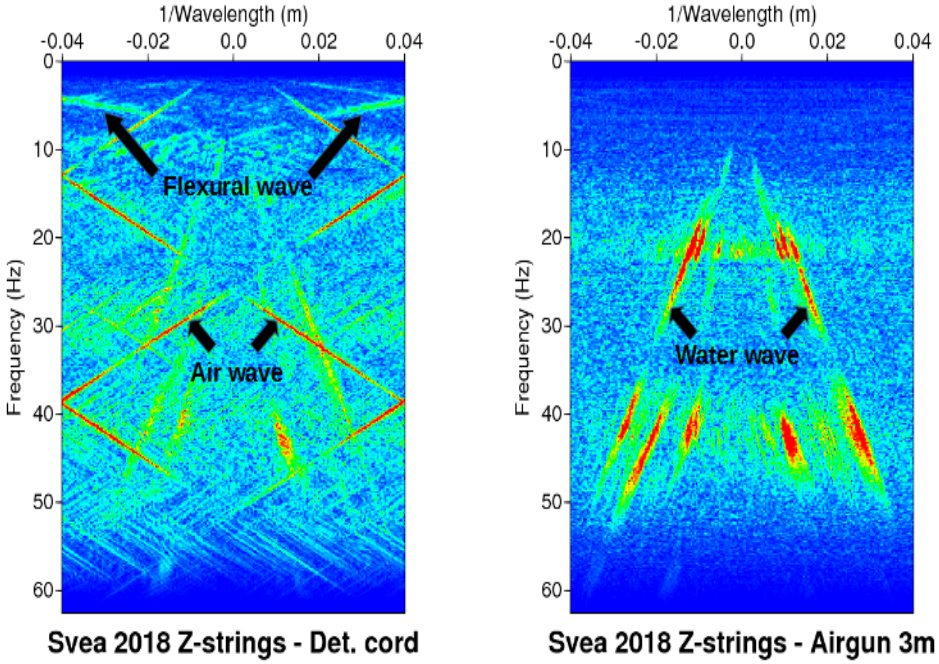

Figure 12. Frequency-wavenumber spectra of split-spread shot gathers using (left) 25 m line source and 12.5 m geophone strings (E12), and (right) single air gun and 12.5 m long geophone strings (E13). The amplitude of the air and flexural waves are very strong using detonating cord as source, and due to the slow velocity and long receiver spacing they are severely spatially aliased. The water wave and reflections (including multiples) are thus clearly revealed when an airgun is used as source.

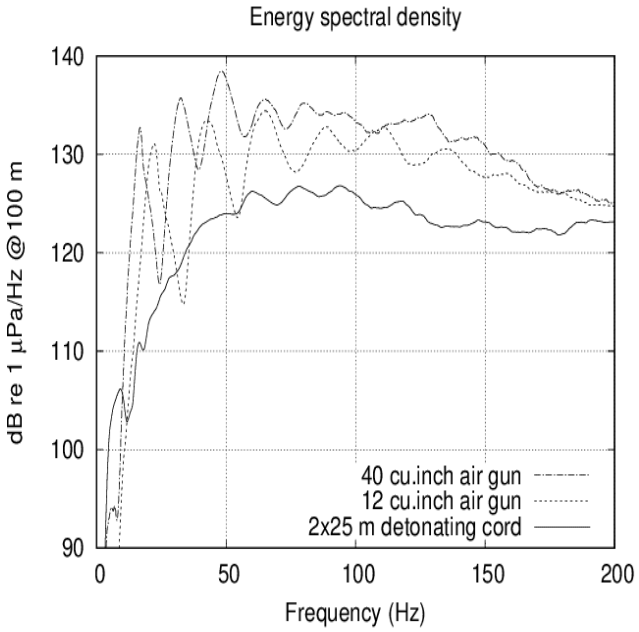

Figure 13. Hydrophone spectra obtained using detonating cord on the ice and two types of air guns deployed at 4 m depth. The hydrophones were deployed at 5 m depth, and the water depth was 20-50 m. The spectra were averaged over many recordings with offsets in the range 90-110 m. The air gun spectra are on average much higher compared with those of the detonating cord, but they are strongly modulated by the bubble pulse and declining above 150 Hz due to source and receiver ghosts. Only for the very low frequency range 3-10 Hz is the detonating cord dominating.

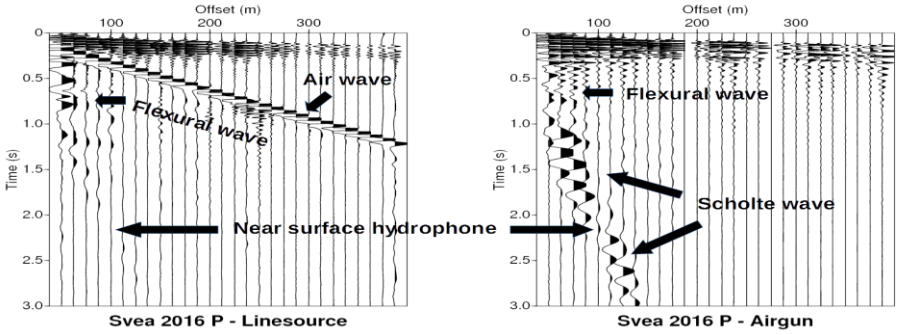

Figure 14. Hydrophone data obtained using (left) detonating cord on the ice (E14) and (right) an air gun at 1.5 m depth (E15). The hydrophones are deployed with varying depth as shown in the lower part of Figure 3. The amplitudes of Scholte waves decay as the distance from the seabed to the hydrophone position increases. Due to the varying depth of the hydrophones, the Scholte wave amplitudes are varying with offset.

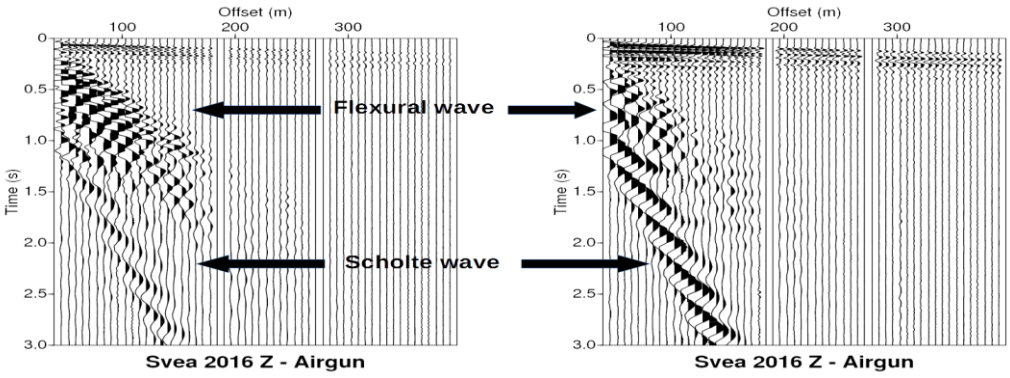

Figure 15. Geophone shot gather using air gun at (left) 1.5 m depth (E16) and (right) 3.0 m depth (E17). When the source is closer to the sea floor (the water depth at the source was only 5 m), the Scholte waves increase in amplitude while the flexural wave amplitudes decrease.

REFERENCES

Aki K. and Richards P. G. 1980. *Quantitative Seismology, Theory and Methods – Volume I.* W. H. Freeman and Company, San Francisco.

Barr F. J., Nyland D. L. and Sitton G. A. 1993. Attenuation of Flexural Ice Waves and Random Noise Using Both Geophones and Hydrophones. *63rd SEG Annual International Meeting*, Expanded Abstracts, P558-561.

Beresford-Smith G. and Rango R. N. 1988. Dispersive Noise Removal in T-X Space: Application to Arctic Data. *Geophysics* **53** (3), 346–58.

Boiero D., Wiarda E. and Vermeer P. 2013. Surface- and Guided-Wave Inversion for near- Surface Modeling in Land and Shallow Marine Seismic Data. *The Leading Edge* **6**, 638–46.

Cremer L., Heckl M. and Petersson B. A. T. 2005. Survey of Wave Types and Characteristics. In: *Structure-Borne Sound*, pp. 27-148. Springer, Berlin, Heidelberg.

Crighton D. G. 1979. The Free and Forced Waves on a Fluid-Loaded Elastic Plate. *Journal of Sound and Vibration* **63** (2), 225–35.

Davidson M. E, Jorgensen P. R., Rosenbladt R. L., Sandroni S., Del Molino G. and Baudo S. 2008. 2007 Arctic on-Ice Seismic Experiment: Operations and Results from a 2D/3D Seismic Program to Investigate Mitigation of the Ice Flexural Wave. 78th *SEG Annual International Meeting,* Expanded Abstracts, P21–24.

Del Molino G., Rovetta D., Mazzucchelli P., Sandroni S., Rizzo F. and Andreoletti C. 2008. Seismic Exploration on Ice: The Flexural Wave Noise Challenge. 78th *SEG Annual International Meeting,* Expanded Abstracts, P2571–75.

Ewing M. and Crary A. P. 1934. Propagation of Elastic Waves in Ice. Part II. *Physics* **5** (7), 181–84.

Ewing M., Crary A. P. and Thorne A. M. 1934. Propagation of Elastic Waves in Ice. Part I. *Physics* **5** (6), 165–68.

Hall K. W., Nieto C. E., Gallant E. V. and Stewart R. R. 2001. Multicomponent Seismic Survey over Ground-Fast and Floating Ice, MacKenzie Delta North West Territories. *CREWES Research Report* 13, 29–45.

Henley D. C. 2006. Attenuating the Ice Flexural Wave on Arctic Seismic Data. *76th SEG Annual International Meeting,* Expanded Abstracts, P2757–61.

Hunkins K. 1960. Seismic Studies of Sea Ice. *Journal of Geophysical Research* **65** (10), 3459–72.

Johansen T. A., Digranes P., Van Schaack M. and Lønne I.. 2003. Seismic Mapping and Modeling of near-Surface Sediments in Polar Areas. *Geophysics* **68** (2), 566–73.

Johansen T. A., Ruud B. O., Bakke N. E., Riste P., Johannessen E. P. and Henningsen T. 2011. Seismic Profiling on Arctic Glaciers. *First Break* **29** (2), 65–71.

Khaidukov V.G., Neklyudov D. A., Silvestrov I. Y., Protasov M. I., Tcheverda V. A., Reshetova G. V. and Landa E. 2016. Enhancement of Seismic Data Gathered by Floating Ice Acquisition: Application of Local Kinematic Attributes. *86th SEG Annual International Meeting,* Expanded Abstracts, P4654–58.

Khaidukov V. G. 2007. Study of Seismic Wave Fields in Transit Zones. *69th EAGE Conference and Exhibition*, Expanded Abstracts.

Kristoffersen Y., Tholfsen A., Hall J. and Stein R. 2016. Scientists Spend Arctic Winter Adrift on Sea

Ice. *Eos* 97.

Kugler S., Bohlen T., Bussat S. and Klein G.. 2005. Variability of Scholte-Wave Dispersion in Shallow-Water Marine Sediments. *Journal of Environmental and Engineering Geophysics* **10** (2), 203–18.

Lamb H. 1889. On the Flexure of an Elastic Plate. *Proceedings of the London Mathematical Society* s1-21 (1), 70–91.

Lamb H. 1917. On Waves in an Elastic Plate. *Proceedings of the Royal Society A: Mathematical, Physical and Engineering Sciences* **93** (648), 114–28.

Lansley R. M., Eilert P. L. and Nyland D. L. 1984. Surface Sources on Floating Ice: The Flexural Ice Wave. *52nd SEG Annual International Meeting,* Expanded Abstracts, P828– 31.

Parrish J., Palm N. and Bell M. 2015. Equalizing sensitivity of transformer coupled hydrophones. 85th *SEG Annual International Meeting,* Expanded Abstracts, P140–4.

Press F. and Ewing M. 1951a. Propagation of Elastic Waves in a Floating Ice Sheet. *Transactions, American Geophysical Union* **32** (5), 673–78.

Press F. and Ewing M. 1951b. Theory of Air-Coupled Flexural Waves. *Journal of Applied Physics* **22** (7), 892–99.

Proubasta D. 1985. Ice Saw – an Incisive Solution to Seismic Noise. *The Leading Edge* **4** (10), 18–23, 82.

Rendleman C. A. and Levin F. K. 1990. Seismic Exploration on a Floating Ice Sheet. *Geophysics* **55** (4), 402–9.

Romanov I.P., Konstantinov Y. B. and Kornilov N. A. 1997. *Ice Drift Stations "North Pole" (1937-1991)*.

Condensed English Version. Gidrometeoizdat.

Rovetta D., Mazzucchelli P., Del Molino G. and Sandroni S. 2009a. Parsimonious Flexural Ice Wave Modelling in Complex Media. *71st EAGE Conference and Exhibition*, Expanded Abstracts.

Rovetta D., Mazzucchelli P., Del Molino G. and Sandroni S. 2009b. Flexural Ice Wave: Modelling by Analytical Approach. *79th SEG Annual International Meeting,* Expanded Abstracts, P2562–66.

Shtivelman V. 2004. Estimating shear wave velocities below the sea bed using surface waves. *Near Surface Geophysics* **22** (2), 241-247.

Sunwall D. A., Speece M. A. and Pekar S. F. 2012. Advances in on-Sea-Ice Seismic Reflection Methods Using an Air Gun: McMurdo Sound, Antarctica. *Geophysics* **77** (1), S19–30.

Trupp R., Hastings J., Cheadle S. and Vesely R. 2009. Seismic in Arctic Environs: Meeting the Challenge. *The Leading Edge* **28** (8), 936–42.

Viktorov I. A. 1967. *Rayleigh and Lamb Waves*. Plenum Press, New York.

Yang T. C. and Yates T. W. 1995. Flexural Waves in a Floating Ice Sheet: Modeling and comparison with Data. *The Journal of the Acoustical Society of America* ***97*** (2), 971–77.